Tectonophysics xxx (2016) xxx–xxx

Contents lists available at ScienceDirect

Tectonophysics

journal homepage: www.elsevier.com/locate/tecto

Geophysical-petrological modelling of the East Greenland Caledonides – Isostatic support from crust and upper mantle

Christian Schiffer [a,c,*], Niels Balling [a], Jörg Ebbing [b], Bo Holm Jacobsen [a], Søren Bom Nielsen [a]

[a] Department of Geoscience, Aarhus University, Høegh-Guldbergs gade 2, DK-8000 Aarhus C, Denmark
[b] Department of Geoscience, Christian-Albrechts-University Kiel, Otto-Hahn-Platz 1, D-24118 Kiel, Germany
[c] Department of Earth Sciences, Durham University, Science Labs, Durham DH1 3LE, UK

A R T I C L E I N F O

Article history:
Received 16 January 2016
Received in revised form 13 May 2016
Accepted 18 June 2016
Available online xxxx

Keywords:
Geophysical-petrological modelling
Gravity-isostatic modelling
Fossil subduction
East Greenland
Caledonides

A B S T R A C T

Teleseismic receiver function analysis imaged a complex upper mantle structure in the Central Fjord Region of East Greenland, including an east-dipping high velocity layer and a mantle wedge of high crustal or low mantle velocities. This was interpreted as a fossil Caledonian subduction complex, including a slab of eclogitised mafic crust and an overlying wedge of serpentinised mantle. In this paper, we use a multi-disciplinary geophysical and petrological modelling approach to test this proposed fossil subduction model.
The consistency of the obtained velocity model with the regional gravity field is tested by forward density modelling and isostatic calculations. The models show that the sub-crustal structure, given by the more buoyant mantle wedge and the dipping high velocity/density layer, yield in a markedly better fit as compared to a homogeneous mantle lithosphere.
Petrological-geophysical modelling is performed by testing different upper mantle compositions with regard to topography, gravity and seismic velocities using Litmod2D. This suggests that the observed lower crustal/uppermost mantle bodies could be a combination of mafic intrusions, serpentinised peridotite and metamorphosed mafic crust. The preferred composition for the dipping structure is eclogitised mafic crust, and hydrated peridotite filling the overlying mantle wedge. Models lacking an eclogite layer or a hydrated upper mantle composition show an inferior fit and, therefore, are not favoured representatives. This supports the interpretation as a fossil subduction zone complex. The spatial relations with Caledonian structures suggest an early Caledonian origin.

1. Introduction

The North Atlantic Realm (NAR) experienced a number of major tectonic events during the past 500 Ma which shaped the present-day topographic and crustal and upper mantle structure of the North Atlantic passive margins. While the general geodynamic evolution is known, various issues are still a matter of discussion. This applies to details of accretionary events associated with the Palaeozoic Caledonian orogeny, deep processes in the mantle related to the formation of the North Atlantic Igneous Province and the present-day state of isostasy of the high topography along the magma-rich passive margins of East Greenland and Scandinavia.

Recently, it has been suggested that remnants of an early Caledonian east-dipping subduction zone are entrained in the lithosphere of the Central Fjord (CF) region of East Greenland (Schiffer et al., 2014, 2015a). Teleseismic receiver functions of the CF array indicate eclogitised mafic crust in the dipping layer and an overlying serpentinised mantle wedge. This structure could be part of a once contiguous eastward dipping Caledonian (or older) subduction zone along the eastern margin of Laurentia, connected with the so-called “Flannan reflector”, offshore northern Scotland (Smythe et al., 1982; Snyder and Flack, 1990; Warner et al., 1996) that shows very similar geometrical and geophysical properties (Schiffer et al., 2015b).

In this study, we will substantiate the interpretation of a fossil subduction zone in East Greenland, by a detailed multi-disciplinary approach, including density, isostatic and petrological modelling. In particular, we will quantitatively differentiate between a set of selected end-member models that include a fossil subduction setting and alternative geometries and compositions.

2. Geological setting

The geological and topographic expression of the North Atlantic Realm (NAR) is considered to be mainly shaped during the past 500 Ma, with the Palaeozoic Caledonian orogeny (circa 425 Ma), rifting, continental break-up accompanied by an extreme magmatic outburst

* Corresponding author at: Department of Earth Sciences, Durham University, Science Labs, Durham DH1 3LE, UK.
E-mail address: christian.schiffer@zoho.com (C. Schiffer).

http://dx.doi.org/10.1016/j.tecto.2016.06.023
0040-1951/© 2016 Elsevier B.V. All rights reserved.

(circa 60 Ma), and the formation of the North Atlantic and its passive continental margins.

2.1. The Caledonian orogeny

The Caledonian orogeny was the consequence of continental drift and resulting collision of three palaeocontinents, Laurentia, Baltica and Avalonia and a number of microcontinents and terranes during the closure of the Iapetus Ocean in the Ordovician to Early Devonian (Cocks and Torsvik, 2011).

The general tectonic development of this Himalayan-type orogeny is understood, but details of timing, direction, location and the number of involved subduction events are unknown. General agreement exists, about an early, east-dipping subduction event along the eastern and southern margin of Laurentia, in the British Caledonides (Grampian phase) and northern Appalachians (Taconian phase), followed by a west-dipping subduction of Iapetus oceanic lithosphere and Baltica beneath Laurentia (Scandian phase) (Karabinos et al., 1998; Dewey, 2005; Leslie et al., 2008; van Staal et al., 2009).

The surface geology is well-studied in Scandinavia (e.g. Gee et al., 2008), which applies also for the ice-free regions in East Greenland (Henriksen, 1999; Henriksen and Higgins, 2008b) and indicates a generally bivergent orogeny (west-vergent in East Greenland and east-vergent in Scandinavia, Roberts, 2003; Gee et al., 2008; Leslie et al., 2008). In East Greenland, the eastern part of the surface geology is dominated by Caledonian thrust sheets lying atop of Archaean basement, while the western part is composite of post-Caledonian sedimentary basins and Tertiary flood basalts and intrusions (Gee et al., 2008; Henriksen and Higgins, 2008b; Gasser, 2013; see Fig. 1). The Caledonian foreland basin and the western Caledonian Deformation Front are exposed in the north and disappear beneath the ice sheet south of 79° N for most of the length of the orogen (Fig. 1).

A large age variation of magmatic and high grade metamorphic rocks from roughly 360 Ma to 500 Ma are indicators for a complex and prolonged orogenic and collisional evolution (Steltenpohl et al., 2003; Gasser, 2013; Corfu et al., 2014, and references therein).

This evidence has led to different tectonic scenarios of the East Greenland and Scandinavian Caledonides, departing from a simple, west-dipping Scandian subduction, including a late eastward intracratonic underthrusting (Gilotti and McClelland, 2011), early west-dipping (Brueckner and van Roermund, 2004; Brueckner, 2006) as well as east-dipping subduction (Roberts, 2003; Gee et al., 2008; Streule et al., 2010).

2.2. Continental break-up and magmatism

A long period of passive lithospheric relaxation and post-orogenic collapse of the Caledonian mountain range followed since the Devonian, reactivating some of the Caledonian faults and adding much complexity to the original Caledonian structures (Andersen et al., 1991; Dewey et al., 1993; Fossen, 2010).

This approximately 340 Ma long lasting period transitioned into active rifting culminating in continental break-up and sea-floor spreading in the early Cenozoic (Skogseid et al., 2000; Nielsen et al., 2007; Gernigon et al., 2015). Break-up was accompanied by a large magmatic outburst, which affected large parts of the NAR, leading to the formation of the North Atlantic Igneous Province and the Iceland Melt Anomaly (Saunders et al., 1997). This magmatic event is commonly associated to the impingement of a mantle plume (e.g., Fitton et al., 1997; Tegner et al., 1998) but also plate tectonic origins are proposed (e.g., Korenaga, 2004; Foulger et al., 2005).

2.3. Present-day passive margins

The magma-rich passive margins along the North Atlantic are accompanied by high topography in East Greenland, Scandinavia and the British Isles. The evolution of this high-elevation, low-relief topography is matter of significant debate (e.g. Nielsen et al., 2009b; Pascal and Olesen, 2009; Chalmers et al., 2010). The occurrence of this distinct topographic expression has been explained by the idea that these landscapes are peneplains created by erosion of ancient topography to sea level and recently uplifted to their present elevation (Japsen and Chalmers, 2000; Lidmar-Bergström and Näslund, 2002). For this uplift a series of processes has been proposed (Doré, 2002), among others, dynamic support from the sub-lithospheric mantle, e.g. by asthenospheric diapirism (Rohrman and van der Beek, 1996). Contrary to this, others favour models where the present topography constitutes remnants of the original Palaeozoic Caledonian mountain

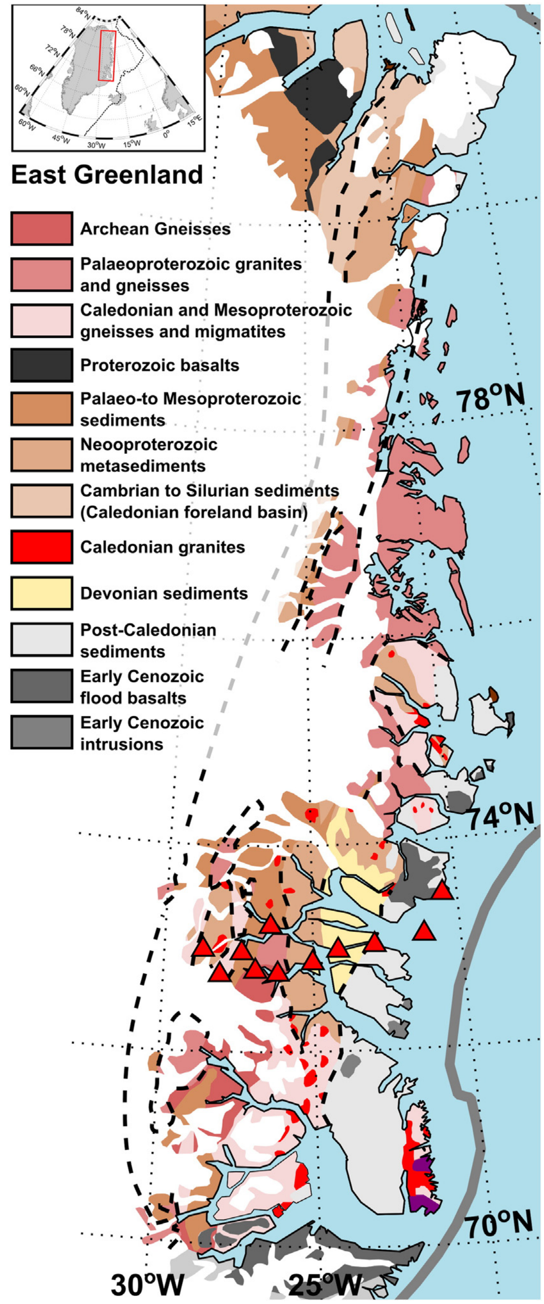

Fig. 1. Geological map of the East Greenland Caledonides (Henriksen, 1999; Henriksen and Higgins, 2008a; Gasser, 2013). Red triangles – locations of the CF array-stations. Stippled black lines – major faults. Thick grey line – continent ocean transition. Inset figure shows an overview of the North Atlantic and the position of the map. (For interpretation of the references to colour in this figure legend, the reader is referred to the web version of this article.)

Please cite this article as: Schiffer, C., et al., Geophysical-petrological modelling of the East Greenland Caledonides – Isostatic support from crust and upper mantle, Tectonophysics (2016), http://dx.doi.org/10.1016/j.tecto.2016.06.023

ranges preserved due to slow, climatically controlled pre-quaternary erosion and faster fjord-incisions during the Quaternary compensated by isostatic rebound (Egholm et al., 2009; Nielsen et al., 2009b; Pedersen et al., 2010).

Densely distributed geophysical studies in Scandinavia have imaged the crustal structure of the Scandinavian Caledonides (see Maupin et al., 2013 and references therein) providing important evidence that the high topography is isostatically supported by thick crust as well as lateral variations of crustal density and lithospheric composition and thickness (Ebbing et al., 2012; Gradmann et al., 2013). This is in general agreement with negative gravity anomalies correlating with high topography (Balling, 1980; Ebbing, 2007).

The much sparser, mainly active source seismic studies in East Greenland do as well indicate thick crust of 40–48 km beneath most the Caledonian high topography from 70° N to 74° N (Voss et al., 2009 and references therein), supported by region-wide gravity analysis (Schmidt-Aursch and Jokat, 2005; Braun et al., 2007) and receiver functions analysis (Dahl-Jensen et al., 2003, p.; Kumar et al., 2007; Schiffer et al., 2015a). Regional surface wave studies using the available permanent stations in Greenland and the surrounding areas provide limited indications for the thickness of the lithosphere (Darbyshire et al., 2004).

Significant parts of the original Caledonian mountains have been eroded, which consequently caused uplift due to isostatic adjustments (Nielsen et al., 2009a; Gołędowski et al., 2013; Medvedev et al., 2013; Medvedev and Hartz, 2015).

3. Gravity and isostasy

Previously published results from receiver function modelling (Schiffer et al., 2015a) will be the base for detailed forward density modelling. Firstly, the available gravity data is shortly described and quality checked (Section 3.1). Then, the residual gravity field will be computed and analysed (Section 3.2). Finally, the gravity response of a set of different forward density models, based on the receiver function results, will be tested (Section 3.3).

3.1. Gravity data

A compilation of gravity data of the Arctic region – ArcGP (Forsberg and Kenyon, 2004; Kenyon et al., 2008) – was used to perform the present study and includes free-air (FA) and Bouguer gravity anomalies (BA). In the study area, the data consist of a large number of onshore measurements supplemented by offshore mapping (Forsberg, 1986; Andersen et al., 2009). The BA is obtained using a Bouguer-plate correction for the topography with a density of 2670 kg/m^3 and a density of 970 kg/m^3 for the ice cover (Gaina et al., 2011), but a terrain correction was not applied. After studying recent available topography models (including ice thickness and bathymetry), we found that a sufficiently detailed terrain correction is not applicable, given the low resolution of the models in the offshore areas. The most advanced available bathymetric model is the IBCAO model (Jakobsson et al., 2012), but the data coverage in the fjords of Central East Greenland is still insufficient.

Eighty-three terrain corrected gravity stations, which were available from Forsberg and Strykowski (pers. Comm., 2008), show terrain corrections of up to 40 mGal. However, most of the terrain corrections show values smaller than 20 mGal and the median is 7.99 mGal. Hence, we expect the BA to be typically 20 mGal too low for single station measurements in rough terrain, much less elsewhere, and mostly affecting short wavelengths (<25 km).

3.2. Isostatic gravity anomaly

We estimated the isostatic gravity residual of the wider study area. For this purpose, we used the topography (ETOPO1, Fig. 2) to calculate an Airy-isostatic Moho depth (Fig. 3b) by weighting the thickness of the ice (density of 970 kg/m^3) and bedrock (2670 kg/m^3) above

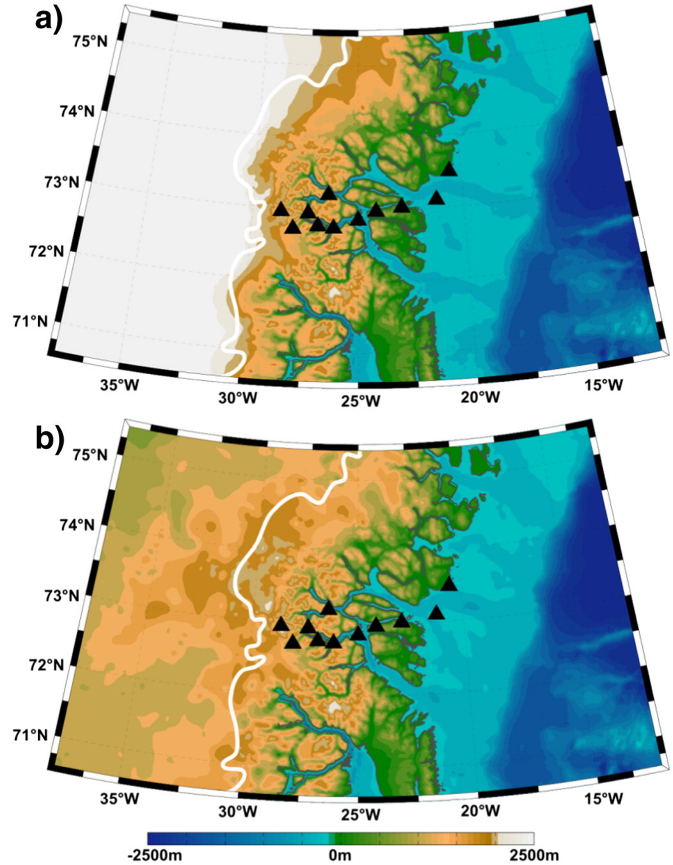

Fig. 2. Topography in the Central Fjord region. (a) topography including ice. (b) topography of the bedrock surface, without ice coverage. White line – edge of the Greenland ice sheet. Black triangles – station positions of the CF seismological array.

sea-level with a crustal root (2800 kg/m^3) with a reference crustal thickness of 35 km and a density contrast of 500 kg/m^3 between crust and mantle. The bedrock topography beneath the ice sheet and the ice thickness is expected to have a rather large uncertainty (20–200 m horizontal and ~1 m vertical for the top ice; 5–50 km horizontal and 10–100 m vertical resolution for the bedrock elevation, http://nsidc.org/). The RMS error of the bedrock topography of the newer model from Bamber et al. (2013) is given at >150 m in East Greenland. The gravity response (*Isoreg*) of this isostatic Moho model was calculated with the software LithoFlex (Braitenberg et al., 2007) using the above mentioned reference crustal thickness and density contrast. The Airy-isostatic Moho was not smoothed and shows high frequent variation corresponding to the topography. However, because of the depth of the Moho, *Isoreg* will be smooth. The isostatic anomaly ($giso_{res}$) is calculated by subtracting *Isoreg* from the observed BA (Fig. 3c).

The isostatic anomaly may mainly reflect non-isostatic sources in the lithosphere and asthenosphere, but also flexural effects and differences in crustal and upper mantle mass distribution not included in this rather simple model. Errors in topography or ice thickness and density will result in a corresponding error in the gravity residual. Therefore, gravity residuals in the area of the ice sheet were not in the scope of our study.

We identify a number of significant features in the estimated gravity isostatic residual (Fig. 3c): (i) a clear negative residual is observed along the approximate extension of the Greenland ice sheet (white line) which we relate to the deflection of the crust and lithosphere due to flexural loading at the edge. (ii) The fjord systems in central East Greenland are clearly not locally isostatically compensated, which is reflected by the strongly negative gravity residuals in the fjords and positive gravity residuals in the surrounding topographic highs, correlated with changes in elevation. The short wavelengths of these anomalies,

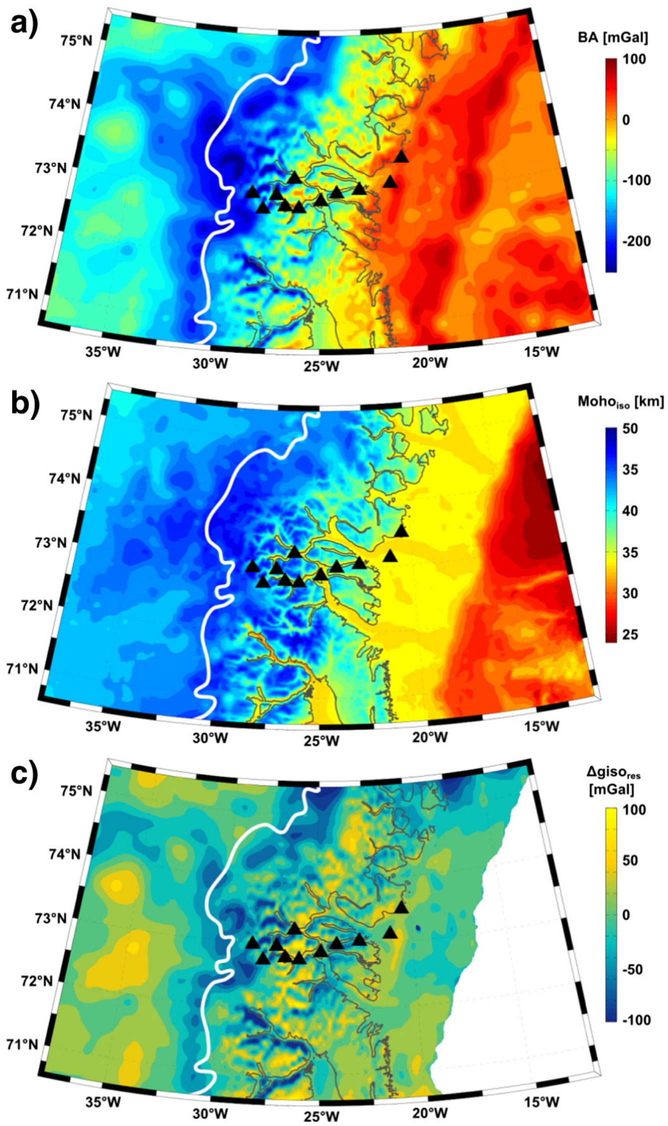

Fig. 3. Gravity and isostasy of the Central Fjord region. (a) observed Bouguer gravity anomaly. (b) isostatic Moho with local compensation of observed topography. See text for details. (c) Isostatic gravity residual. White line – edge of the Greenland ice sheet. Oceanic domain is cut out. Black triangles – station positions of the CF array.

well below 50 km, are the reason why the topography probably is carried mostly by the stiff lithosphere. (iii) An area of ~50–100 km width of outstanding higher residuals can be identified situated almost coast-parallel, starting at ~27° W in the south (71° N) and at ~22° W in the north (75° N). A reason could be high densities of the rocks in this area, which consists of gneisses, granites and old metasediments. (iv) Similarly, an area of isostatic anomaly lows is situated directly to the east and extending from ~72–73° N. The location of this anomaly corresponds rather well with the Devonian basin (cf. Fig. 1), which might be causing the isostatic anomaly.

Despite the mentioned distinct zones of high (both negative and positive) isostatic anomalies, the general regional trend is close to zero indicating close to isostatic compensation of long wavelength topographic features.

3.3. Density and isostatic modelling

Density modelling was performed with the software IGMAS+ (Schmidt et al., 2010). Similar to Schiffer et al. (2015a), we averaged the BA over a distance of 25 km to the north and south of the defined position of the CF array in order to assess the 2D regional gravity field. This averaging also decreases the error of the missing terrain correction. The resulting averaged BA shows a clear trend starting at circa −200 mGal in the west and gradually increasing to +50 mGal in the eastern end of the profile, close to the coast line. The central part of the CF array comprises a close to constant BA at −50 mGal along a ~75 km wide segment. The topography was averaged, accordingly, and the ice column was replaced by the same mass of rock column at 2670 kg/m^3 density, because the software Litmod2D does not allow an ice layer in the model. Including this “rock-for-ice masses”, topography reaches a maximum of approx. 1700 m in the west (100–200 m of replaced ice cover) and decreases almost linearly to sea-level in the eastern end of the profile.

Schiffer et al. (2015a) presented a first-order test of the obtained P-wave velocity model (Fig. 4a), by directly translating P-wave velocities to densities using the Nafe-Drake relation. The calculated gravity response is in good agreement with the observed data, however, as to be expected, some variations and local anomalies were not recovered, such as the steeper gradients around the flanks of the profile as well as the flat BA in the central part.

Based on this preliminary model, we performed a more detailed gravity-isostatic analysis. We produced two forward models, which were based on the obtained receiver function model and corresponding densities. The models are constructed with a number of polygons, each with constant density. Layer boundaries and shape of the polygons were chosen in accordance with the seismic velocity models. The 2.5D model of about 255 km length was extrapolated with 500 km in all lateral directions in order to avoid edge effects. Gravity and topography data were prepared in an area 150 km around the extent of the CF array (see Fig. 4b–c, lowermost panels). The whole density structure along this entire approx. 555 km long profile was modelled, with the seismological receiver functions providing constraints only in the central 255 km part (Fig. 4, second panel from bottom). The initial reference model consists of polygons with constant densities, such as different sedimentary layers (metasediments – 2650 kg/m^3, older sediments – 2550 kg/m^3 and younger sediments – 2250–2450 kg/m^3), upper crust (2750 kg/m^3) and lower crust (2950 kg/m^3), as well as three layers in the mantle wedge with successively increasing density (3100 kg/m^3, 3200 kg/m3 and 3300 kg/m^3), a high density dipping slab (3400 kg/m^3) and finally continental (3350 kg/m^3) and oceanic mantle lithosphere (3325 kg/m^3) and asthenosphere (3300 kg/m^3) (see Table 1).

When, after some adjustments (see below), a model fulfilled the observed BA, its isostatic topographic response was calculated (Fig. 4, upper panel, stippled red lines), balanced with a reference model. For the isostatic model, the density structure was averaged over a lateral moving window 50 km width. The reference model consisted of a pure asthenosphere below a layer of 2500 m of air (“free asthenospheric surface”) (Lachenbruch and Morgan, 1990).

The first forward model (Fig. 4b) comprises all structural elements and the geometry followed the receiver function velocity models. Uncertainty in the receiver function modelling and interpolation between the stations translates into the density model. Not many adjustments were necessary to obtain a good fit between observed and modelled gravity (Fig. 4b). The depth of the lithosphere-asthenosphere-boundary (LAB) was chosen at 175 km in the west, in general agreement with seismological results, (e.g. Darbyshire et al., 2004; Conrad and Lithgow-Bertelloni, 2006), decreasing towards the coastline. This LAB depth decrease and the introduction of a slightly less dense “oceanic” lithosphere clearly facilitates fitting the observed regional gravity trend. The resultant model shows that no substantial adjustments to the initial receiver function based model have to be applied to describe the regional gravity field (Fig. 4b, second row).

In the second forward model all “sub-crustal elements” were removed (Fig. 4d, third and fourth row). Much more substantial crustal adjustments were needed in order to make this model alternative fitting

Please cite this article as: Schiffer, C., et al., Geophysical-petrological modelling of the East Greenland Caledonides – Isostatic support from crust and upper mantle, Tectonophysics (2016), http://dx.doi.org/10.1016/j.tecto.2016.06.023

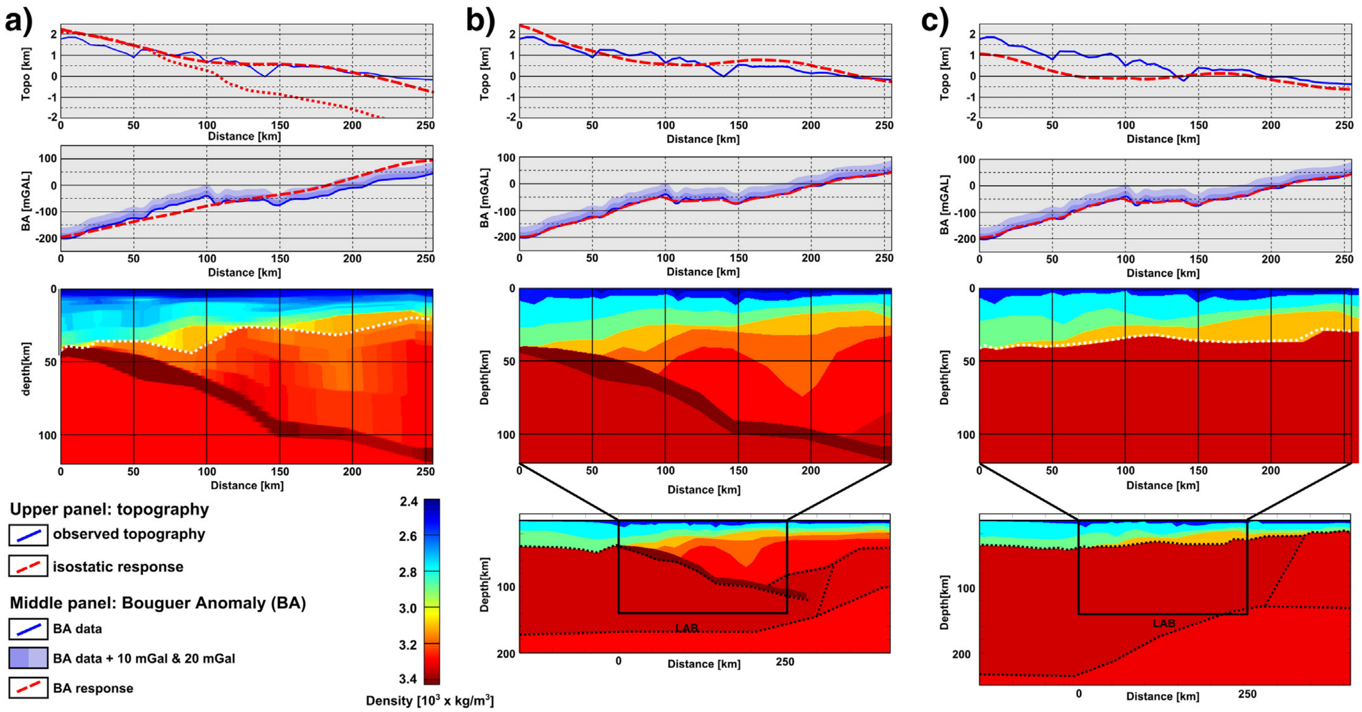

Fig. 4. Results from IGMAS + density and isostatic modelling. 1st from above: topography observed (blue) and isostatic response of the model (stippled red). 2nd from above: Bouguer gravity anomaly, observed (blue) and modelled (red). Blue shading indicates the BA data plus 10 and 20 mGal to illustrate the possible terrain correction error. 3rd from above: density model of the key section. White dotted lines illustrate the Moho interpretation. 4th from above: whole model. Black box shows the section of the CF array. (a) The directly Vp-to-rho converted receiver function model. (b) Forward model containing all elements from the receiver function geometry. (For interpretation of the references to colour in this figure legend, the reader is referred to the web version of this article.)

the observed gravity. Also, the lithospheric structure was changed, now with a very steep gradient of 100 km depth change over a horizontal distance 250 km, in order to fit the regional gravity trend.

The isostatic test shows that the complex upper mantle structure, including a more buoyant upper mantle wedge is in good agreement with topography and gravity field (Fig. 4b). The model lacking the sub-crustal complexity shows a substantially worse topographic response, when the gravity field is fitted (Fig. 4c).

4. Geophysical-petrological modelling

Although receiver function and density modelling are consistent with substantial heterogeneity in the upper mantle, the question remains what these density and velocity structures may represent in terms of lithology and composition at relevant P-T conditions.

We used Litmod2D (Afonso et al., 2008) to perform a number of tests addressing this question. Initially, 2D structures were defined, that represent different lithologies and we defined these close to the obtained receiver function and IGMAS + models. The models were limited to a resolution of 1 km. Each defined model structure was assigned a lithology as well as thermal parameters (thermal conductivity and thermal expansion coefficient, and their temperature dependence). Litmod2D calculates the steady state temperature field, with the LAB defined as the 1300 °C isotherm. Through pre-defined P-T phase diagrams for the defined compositions, and with the resulting temperature and pressure fields, model densities and seismic velocities are derived. The phase diagrams were calculated with PERPL_EX (Connolly, 1990, www.perplex.ethz.ch) using the data base from Holland and Powell (1998), which also allows hydrous compositions. Model layers may also be assigned constant densities, independent of composition.

Table 1
Lithologies and densities used for the gravity-isostatic modelling.

	Lithology	ρ [kg m^{-3}]
Sediments	Mesozoic shallow	2250
	Mesozoic deeper	2450
	Devonian	2550
	Metasediments	2650
Crust	Upper	2750
	Lower	2950
Sub-crustal	Mantle wedge, upper	3100
	Mantle wedge, middle	3200
	Mantle wedge, lower	3300
	Eclogite	3400
Lithosphere	Continental	3350
	Transitional	3325
Asthenosphere	Reference	3300

4.1. Model structure

Similar to the IGMAS + gravity modelling, we defined a wide study area, extending 150 km west and east from the original CF array (Fig. 5a), still with main emphasis on the central part along the CF array (Fig. 5b). Here, model geometries were based on the seismological observations, while, towards model boundaries, these structures were simply laterally extended. Since our petrological analysis is focussed on the upper mantle, we defined crustal layers with constant densities: one sedimentary/metasedimentary layer, upper crust, lower crust, and an additional lower crustal layer in the craton west of the study area (Fig. 5a and Table 2). All other deeper structures, including upper, middle and lower mantle wedge layers, the dipping high velocity layer and two different lithospheric geometries (west and east, see Fig. 5a), were assigned compositions coupled to phase diagrams. The tested models were primarily evaluated by the modelled seismic velocities in comparison with those observed, as well as by the isostatic topographic and BA response. Litmod2D also computes FA responses, which were included as a weaker secondary constraint.

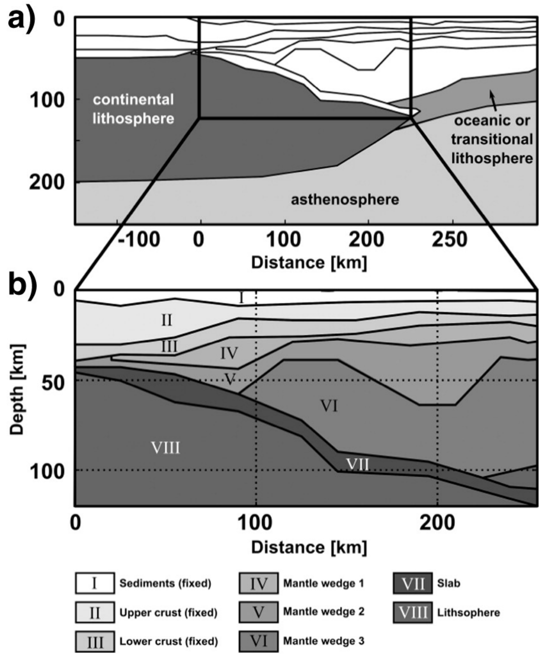

Fig. 5. Model set up for the integrated petrological-geophysical modelling (Litmod2D). (a) Overview of the whole model section, with emphasis on mantle structure. We distinguish between a continental lithosphere beneath the Greenland landmass and a transitional lithosphere further east, while approaching the continent-ocean-boundary. (b) Detailed model section with emphasis on the lithospheric structure. Eight different structural elements (I–VIII) are defined to represent the obtained velocity structure in the Central Fjord region and which are tested with different compositions. I–III are sedimentary and crustal layers, which will comprise fixed, pre-defined densities, not exposed to phase diagrams. IV–VIII are sub-crustal structures, which are tested with different lithologies (see Table 3).

4.2. Model compositions

Table 2, item 5 to 14 specify 10 different lithologies from which we selected five at a time to fill each of the model zones IV to VIII (Fig. 5). First, revisiting Anderson (2007), Christensen and Mooney (1995) and Christensen (1996), we considered possible compositions often discussed in relation to the observed seismic velocities. P-wave velocities of 7.3–7.8 km/s and S-wave velocities of 4.0–4.4 km/s in the mantle may represent compositions which include hydrated and partly serpentinised mantle, partly eclogitised mafic crust as well as intruded lower crust. “Dry” mantle lithologies can in principle also show seismic velocities of down to Vp ≈ 7.7 (Vs ≈ 4.4), such as pyroxene rich mantle compositions. However, this only represents the upper limit of the observed velocities in the mantle wedge. The presence of melts was not considered because of the absence of any present-day active volcanism in the CF region.

We tested a number of different compositions that might be feasible for more accurate tests. We investigated the role of serpentinite and added gradually more water to a Phanerozoic mantle composition (Afonso et al., 2008), while an average serpentinite composition was assumed (Miyashiro et al., 1969; Deschamps et al., 2013). Adding successively less serpentinite to the mantle from top to bottom (e.g. 25%, 20%, 10%, corresponding to a water content of 2.9%, 2.3% and 1.2%) was able to produce the observed velocity ranges. We also tested different crustal compositions that might have been exposed to eclogitisation and found that the lower crustal composition suggested by Rudnick and Gao (2003) yields a good fit. Finally, we tested a number of mantle compositions to obtain low seismic velocities. This showed that the only tested composition which was able to explain the required low mantle velocities, without having very high densities, was a mixed composition of clinopyroxene (Cpx) and magnesium (Mg)-rich olivine (forsterite, Ol).

Then, we tested numerous different mafic crustal compositions, basalts as well as eclogite compositions found in the North Atlantic region (Bryhni et al., 1969; Mysen and Heier, 1972; Mørk, 1986; Markl and Bucher, 1997), which might produce velocities similar to those observed in the dipping slab. These tests showed that an aluminium- and thereby garnet-rich composition is sufficient to create the high velocities. Also different mantle compositions were tested, where many were rejected, mainly because of unrealistic densities, and we finally chose a harzburgitic composition (Xu et al., 2008) to represent mantle with seismic velocities larger than normal (>8.3 km/s). Unless described otherwise, the standard lithospheric composition was chosen as a standard “Proton” (Proterozoic lithosphere), beneath the western part of the study area (Fig. 5) and as a standard “Tecton” (Phanerozoic lithosphere, Afonso et al., 2008) beneath the eastern part that forms the transition to the ocean (Fig. 5a). Table 2 shows the resulting short-list of composition candidates for the sub-crustal structures.

4.3. Forward modelling

The Litmod2D modelling proceeded in two stages. In stage 1 we fixed model geometries and tested 12 different combinations of lithologies from Table 2. In stage 2 we selected the 6 most promising combinations of lithologies for which the layer boundaries were then adjusted to improve the fit of the isostatic topography response.

4.3.1. Stage 1 – test of principle compositions and combinations

In the first modelling stage the model geometry, based on the receiver function results, was fixed. Densities and velocities in the crustal layers

Table 2
Tested lithologies in the integrated petrological-geophysical modelling. Sediments and crustal layers comprise pre-defined homogeneous densities and are not calculated after P-T phase diagrams, as all other lithologies.

	Lithology	SiO_2	Al_2O_3	FeO	MgO	CaO	Na_2O	K_2O	H_2O	A [10^{-6} Wm^{-3}]	λ [Wm^{-1} K^{-1}]	α [10^{-5} K^{-1}]	ρ [10^3 kg m^{-3}]
1	Sediments	–	–	–	–	–	–	–	–	0.500	2.0	2.5	2.55/2.65
2	Upper crust	–	–	–	–	–	–	–	–	1.500	2.4	2.2	2.75
3	Lower crust	–	–	–	–	–	–	–	–	0.400	2.0	2.0	2.90
4	LCL (craton)	–	–	–	–	–	–	–	–	0.400	2.0	2.0	3.00
5	Mafic crust	53.4	16.9	8.57	7.24	9.59	2.65	0.62	0.00	0.050	2.6	2.1	–
6	Wet mantle 1	43.0	2.7	6.6	39.1	2.2	0.23	0.01	2.92	0.010	3.2	2.1	–
7	Wet mantle 2	43.3	2.8	6.9	39.4	2.3	0.23	0.01	2.34	0.010	3.3	2.2	–
8	Wet mantle 3	43.8	2.9	7.6	39.8	2.5	0.23	0.00	1.16	0.005	3.4	2.3	–
9	Cpx-Ol rich mantle	48.0	3.6	8.2	28.1	10.0	1.1	0.00	0.00	0.005	3.4	2.3	–
10	Eclogite	47.0	18.0	8.0	11.0	11.0	2.2	0.40	0.00	0.050	2.0	2.0	–
11	Proton	44.6	1.9	7.9	42.6	1.7	0.12	0.00	0.00	0.001	3.5	2.4	–
12	Harzburgite	36.0	0.6	6.0	56.5	0.8	0.0	0.00	0.00	0.001	3.5	2.4	–
13	Tecton	44.5	3.5	8.0	39.8	3.1	0.24	0.00	0.00	0.005	3.4	2.3	–

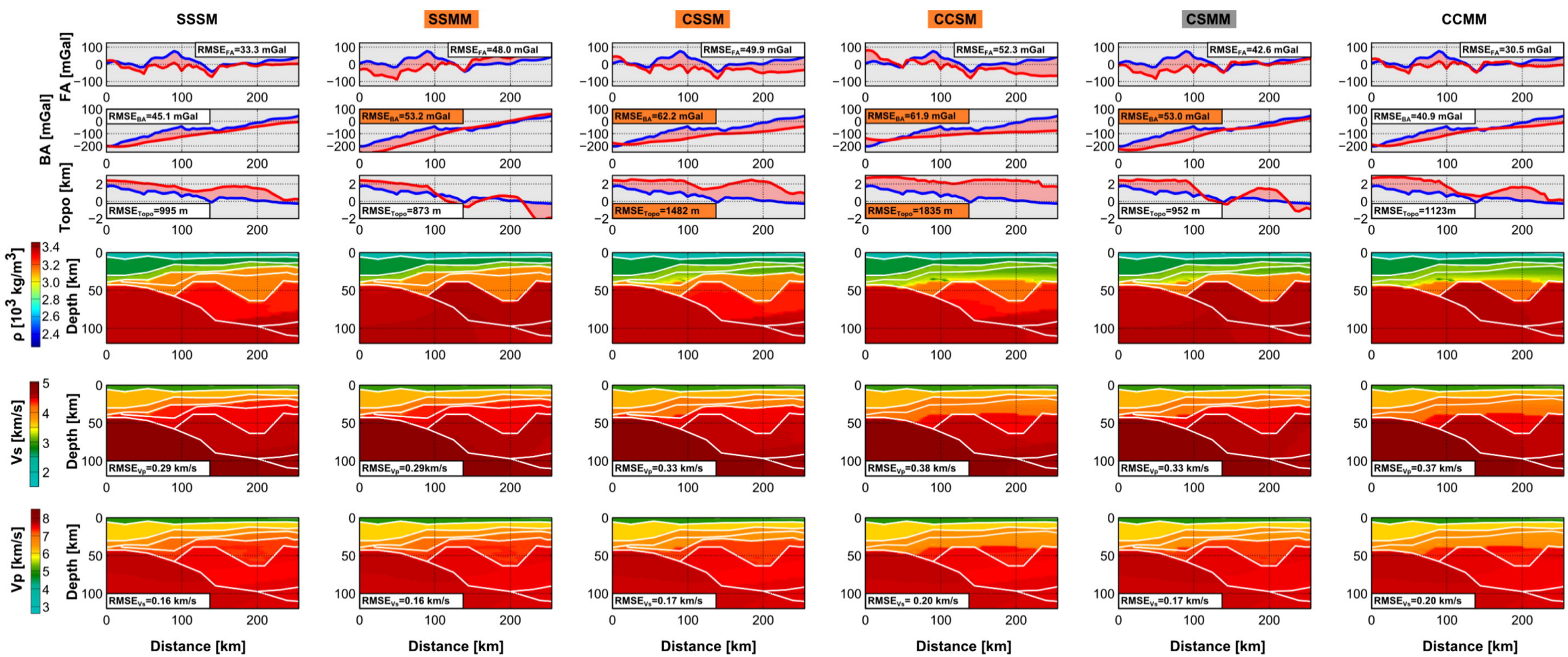

Fig. 6. Results of the first test for combinations without eclogite in the dipping structure. Panels successively from top to bottom: FA [mGal], BA [mGal], topography [km], densities [kg/m^3], Vp [km/s], Vs [km/s]. Blue lines show observed data; red lines show modelled values; red shading emphasises model differences; insets in the corners of each plot show the RMSE of each comparable data set. Green indicates the best fitting models; orange indicates rejection of the model because of a high misfit of this quantity. (For interpretation of the references to colour in this figure legend, the reader is referred to the web version of this article.)

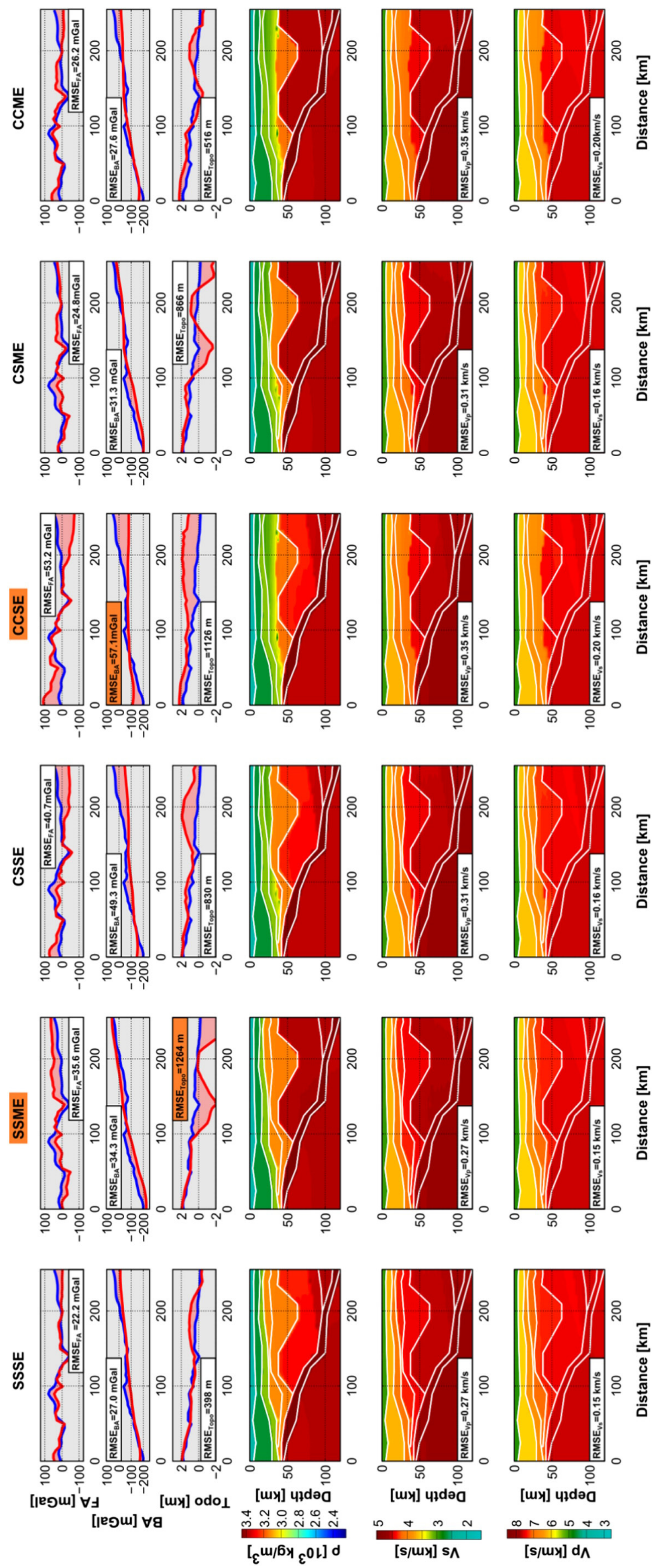

Fig. 7. Results of the first test for combinations with an eclogite layer. Otherwise, same as Fig. 6.

Please cite this article as: Schiffer, C., et al., Geophysical-petrological modelling of the East Greenland Caledonides – Isostatic support from crust and upper mantle, Tectonophysics (2016), http://dx.doi.org/10.1016/j.tecto.2016.06.023

(Fig. 5, items I–III) were fixed as well, as defined in Table 2 (items 1–4). Lithologies in the deeper layers were combined systematically as follows. Structural element IV: Mafic crust (indicated by "C") or wet mantle 1 ("S"). Element V: Mafic crust ("C") or wet mantle 2 ("S"). Element VI: Wet mantle 3 ("S") or Cpx-Ol ("M"). Element VII + VIII: Eclogite over Proterozoic type mantle ("E") or both harzburgite ("M"). Each such model is abbreviated with the corresponding letters in elements IV–VII. SSSE, for instance, indicates a model with three hydrated mantle layers in elements IV–VI and an eclogite layer (VII) above lithosphere (VIII). From these 16 possible combinations we ruled out combinations that consist of hydrated mantle above mafic crust in the elements IV–VI (mantle wedge), which does not make tectonically sense.

The remaining 12 combinations and their model result are shown in Fig. 6 (without eclogite composition in the dipping layer) and Fig. 7 (with eclogite) and are summarised in Table 3 together with the resulting misfits between Litmod2D-predictions and observed Bouguer gravity, observed topography, and the seismologically derived P- and S-velocities (Vp and Vs). The misfit is measured by the root mean square error of individual parameter p ($RMSE = \sqrt{1/n\sum(p_{obs}-p_{calc})^2}$). The RMSE differs strongly between the models, but less for seismic velocities because the lithologies were chosen accordingly. Orange shading shows rejected models due to violations of a chosen gravity misfit <50 mGal and/or topography misfit <1000 m.

Models comprising a layer of eclogite show a generally better fit than models without (Table 3, orange rejected models and rejection criterion). No clear pattern can be observed with regard to the composition of the "mantle wedge", where mafic crust, hydrated mantle and "slow" mantle all may be plausible candidates. The best fitting model comprises differently hydrated mantle layers in the mantle wedge and eclogitised dipping layer (model SSSE).

4.3.2. Stage 2 – model optimisation

In the second stage, we focussed on improving the fit to gravity and especially, to topography. This was performed by adjusting layer boundaries and also by allowing a change of crustal densities within the moderate limits of ± 50 kg/m^3. We performed these adjustments to the 6 models which were not rejected after the first stage (Table 3).

The results of this second stage modelling are shown in Fig. 8 and Table 4. The topography, which was mainly optimised by the modelling, shows very low (<100 m) RMSE for all models. The RMSEs of the other quantities (BA, FA, Vs, Vp) isolate two models that show a superior fit – SSSE′ and CSSE′. Model SSSE′ comprises hydrated mantle peridotite in the mantle wedge (IV–VI) and eclogite in the dipping structure (VII) and shows the best fit to the seismic velocities and also a small error of the gravity response. Model CSSE′, where the uppermost mantle wedge layer (IV) is substituted with mafic lower crust, shows less well

Table 3
Tested model combinations and their RMSE with regard to observed data for test 1. Latin numbers indicate the structure (see Fig. 5). Arabic numbers indicate the tested lithology (see Table 2). Model codes indicate the composition in layers IV–VII. S: serpentinite (or wet mantle); C: crust; M: dry mantle; E: eclogite. The fit to the seismological receiver-function based velocities is uniformly good because candidate lithologies were selected so. The fit to Bouguer gravity ($RMSE_{BA}$) and topography ($RMSE_{Topo}$) differs strongly. Orange shading shows rejected models due to violations of gravity with misfit larger than 50 mGal and/or topography with misfit larger than 1000 m (see Figs. 6 and 7).

	Model	I	II	III	IV	V	VI	VII	VIII	$RMSE_{BA}$ [mGal]	$RMSE_{Topo}$ [m]	$RMSE_{Vp}$ [km/s]	$RMSE_{Vs}$ [km/s]
No eclogite	SSSM	1	2	3	6	7	8	12	12	45.1	995	0.29	0.16
	SSMM	1	2	3	6	7	9	12	12	53.2	873	0.29	0.16
	CSSM	1	2	3	5	7	8	12	12	62.2	1482	0.33	0.17
	CCSM	1	2	3	5	5	8	12	12	61.9	1835	0.38	0.20
	CSMM	1	2	3	5	7	9	12	12	56.0	952	0.33	0.17
	CCMM	1	2	3	5	5	9	12	12	40.9	1123	0.37	0.20
With eclogite	SSSE	1	2	3	6	7	8	10	11	27.0	398	0.27	0.15
	SSME	1	2	3	6	7	8	10	11	34.3	1264	0.27	0.15
	CSSE	1	2	3	5	7	9	10	11	29.3	830	0.31	0.16
	CCSE	1	2	3	5	5	8	10	11	57.1	1126	0.35	0.20
	CSME	1	2	3	5	7	9	10	11	31.3	866	0.31	0.16
	CCME	1	2	3	5	5	9	10	11	27.6	516	0.35	0.20

Please cite this article as: Schiffer, C., et al., Geophysical-petrological modelling of the East Greenland Caledonides – Isostatic support from crust and upper mantle, Tectonophysics (2016), http://dx.doi.org/10.1016/j.tecto.2016.06.023

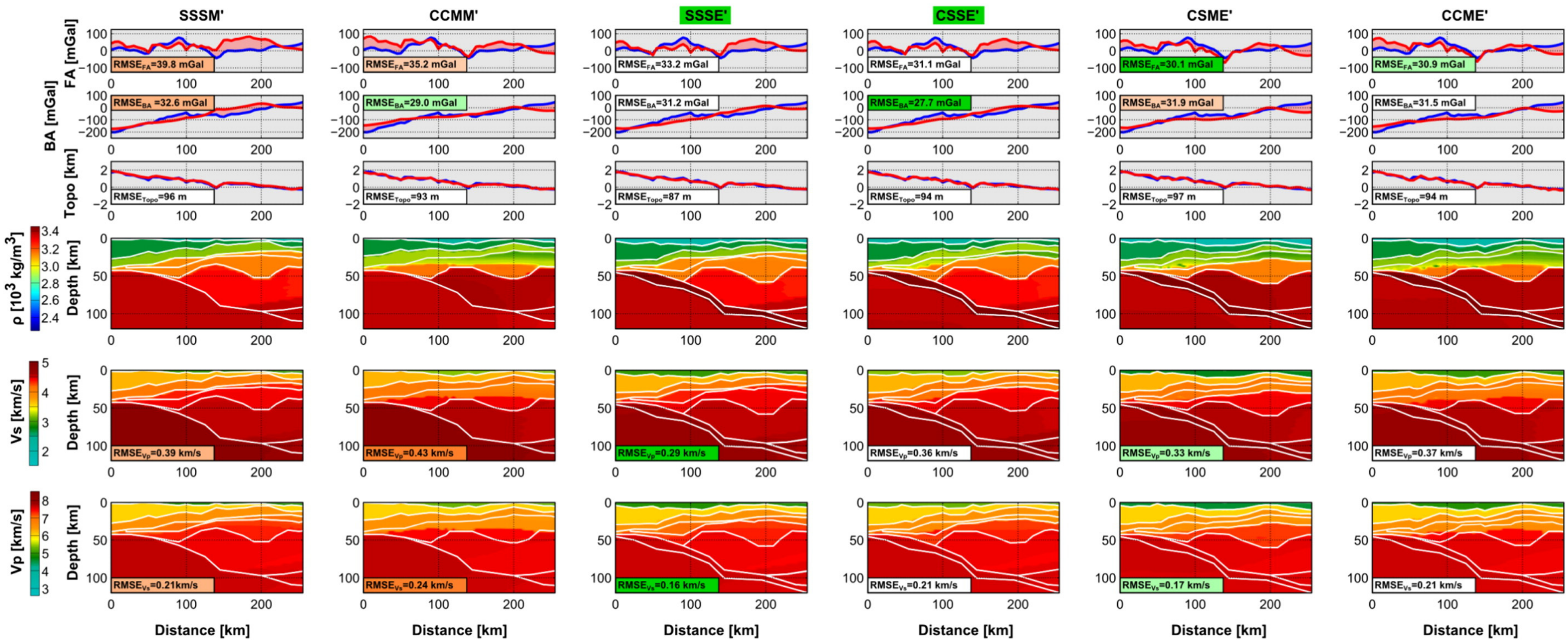

Fig. 8. Results of the second test. The models are based on the not rejected petrological combinations of test 1 (Figs. 6 and 7, Table 4), but were adjusted mostly in the geometry of the layer interfaces to fit topography sufficiently well. Light green shading: second best model results; light orange shading: second worst model results. Otherwise, same as Fig. 6. (For interpretation of the references to colour in this figure legend, the reader is referred to the web version of this article.)

Table 4
Tested model combinations and their RMSE with regard to observed data for test 2. Roman numbers indicate the structure (see Fig. 5a). Arabic numbers indicate the tested lithology (see Table 2). Model codes indicate the composition in layers IV–VII. S: serpentinite (or wet mantle); C: crust; M: dry mantle; E: eclogite. Red shading shows the worst data fit and orange the second worst RMSE of the tested model. Dark green shading shows the best RMSE and light green shading second best RMSE of the tested models.

Model	I	II	III	IV	V	VI	VII	VIII	$RMSE_{Topo}$	$RMSE_{BA}$	$RMSE_{Vp}$	$RMSE_{Vs}$
SSSM′	1	2	3	6	7	9	12	12	96	32.6	0.39	0.21
CCMM′	1	2	3	5	7	9	12	12	93	29.0	0.43	0.24
SSSE′	1	2	3	6	7	8	10	11	87	31.2	0.29	0.16
CSSE′	1	2	3	5	7	9	10	11	95	27.7	0.36	0.21
CSME′	1	2	3	5	7	9	10	11	97	31.9	0.33	0.17
CCME′	1	2	3	5	5	9	10	11	94	31.5	0.37	0.21

fitting seismic velocities but obtains the best fit for the gravity. The model with the largest misfits is SSSM′, which shows an especially poor fit of the gravity data. The gravity of CCMM′ fits the observations rather well, but the seismic velocities are poorly recovered. Thus we deem models SSSM′ and CCMM′ as unlikely representatives of the upper mantle structure of the CF region. Both models have no eclogite slab, which is strong support for the presence of such a structure.

The models CSME′ and CCME′ show varying but overall acceptable data fit. Model CSME′ has a close to average gravity response fit, but good fit to seismic velocities, while model CCME′ shows about average fit for all data sets. Model CSME′ has mafic crust and hydrated mantle in the upper two mantle wedge layers (IV–V) on top of "dry mantle" (VI) with a slab of eclogitised crust. Model CCME′ is similar to CSME′, but comprises mafic crustal composition also in the middle mantle wedge layer (V). We deem these two models to be acceptable, but not favourable representatives of this region. In case higher temperatures are present, a phase transition, now at 40 km depth, might be shallower, which could result in a much better fit of these models (Fig. 8, CCME′ in the density, Vs and Vp plots).

We suggest that a combination of both favoured models, SSSE′ and CSSE′, and possibly an additional different lithospheric composition in the eastern part of the profile (models CSME′ and CCME′) might be a realistic representation of the subsurface in the study area. Hence, the uppermost mantle wedge layer may represent a physically or compositionally mixed structure. The lower continental crust may continue to slightly larger depths than assumed in our model or it has experienced some physical alternation and/or chemical exchange with the underlying serpentinised mantle.

5. Discussion

Analysis of the gravity field in central East Greenland reveals that the area is close to isoststic compensation on a large scale, whereas small-scale topograpohic features, such as the short-wavelength fjords and highs are clearly not in local isostatic equilibrium. Forward density modelling shows that the upper mantle complexity in the central East Greenland Caledonides suggested by receiver function analysis is agreeable to the gravity field. All structural elements, suggestive of a fossil subduction zone complex, obtain a notably better fit as compared to a model comprising only crustal layers atop of a homogeneous mantle lithosphere. The RMSE of the isostatic topography response is estimated at 281 m suggestive of a limited present-day dynamic support from sub-lithospheric sources, in agreement with a recent estimate of <300 m of dynamic support in the East Greenland Caledonides (Schiffer and Nielsen, 2016). Another important result is that the crust alone is insufficient to support the topography in the eastern part of the CF array, close to the coastline. Here additional buoyancy from the low-density mantle wedge is present, while to the west the high topography seems to be compensated by the ~40 km thick crust.

In our model, local isostasy is assumed with a 50 km smoothed topographic response. This is a simplification, and some regional, flexural components may exist. Glacial isostatic adjustment of the present ice sheet will have an effect on the regional isostatic state in East Greenland. However, our assumptions seem to provide a good first order estimate of the main isostatic components along our profile. A study, addressing the geodynamic, thermal and isostatic evolution of the study region, including the proposed slab, from its emplacement, over rifting and continental break-up to the present day, could give further insight into this question.

Integrated petrological-geophysical modelling showed which compositions might be associated to the seismologically obtained velocities and associated densities. Two models were favoured (SSSE′ and CSSE′) and another two models also showed satisfying results (CSME′ and CCME′). We suggest that a combination of the two best models, possibly in addition to two different lithospheric compositions in the west and east of the dipping structure, is the most favourable solution.

The high velocity lower crustal units probably require partly eclogitisation or igneous intrusions, or both. The igneous activity might be the consequence of melting in a subduction setting or during rifting and continental break-up. Lower crustal bodies have been attributed to a number of different rocks and mechanisms. One assumed model is magmatic underplating or the emplacement of lower crustal intrusions associated to rifting (Mjelde et al., 2002; Thybo and Artemieva, 2013), as commonly suggested for the East Greenland margin (Voss et al., 2009 and references therein). Such early Cenozoic, break-up related lower crustal igneous intrusions may have caused vertical movements during emplacement and the subsequent isostatic readjustment of the crust. However, also serpentinite bodies, now entrained into the lower crust, are suggested for parts of the North Atlantic passive margins, commonly interpreted to be formed during syn-rift mantle hydration (Osmundsen and Ebbing, 2008; Reynisson et al., 2010; Lundin and Doré, 2011; Peron-Pinvidic et al., 2013; Rüpke et al., 2013). In a strict sense, these would not be lower crustal bodies, but since they often are indistinguishable from metamorphosed or intruded lower crust, we will still use this expression for simplicity. Also, older inherited pre-rift structures have been proposed in this discussion, such as metamorphosed crust, older igneous intrusions or serpentinite bodies of, for instance, Caledonian age (Gernigon et al., 2004; Fichler et al., 2011; Mjelde et al., 2013). Recent studies suggest, that the lower crustal bodies at the Norwegian margin are a combination of multiple of the proposed models, often showing differences between distal and proximal margin domains (Mjelde et al., 2013; Nirrengarten et al., 2014). Therefore, our preferred model includes lower crustal bodies of physically or chemically mixed serpentinised mantle and metamorphosed crustal bodies, and mafic intrusions. Details of the exact structure, extent and relative amount of the potential compositions in this layer remain uncertain, given the limited resolution of the receiver function image.

The high velocities in the dipping structure may be explained by eclogitised, mafic crust, which can explain the apparent velocity increase at the upper interface as well as the drop at the lower interface. A different mantle composition with higher seismic velocities is possible, but is lacking an explanation for the additional velocity drop, which cannot be sufficiently recovered by thermal effects.

Beneath the crust, to different degrees hydrated and serpentinised mantle wedge is favoured, which fills the space between the crust and a dipping layer of eclogitised mafic crust (Fig. 9). The low seismic velocities may be additionally attributed to a different lithospheric composition.

The presented model alternatives do support the existence of a subduction, collision and/or suture zone between two different continental lithospheric blocks. The observed geophysical properties

Please cite this article as: Schiffer, C., et al., Geophysical-petrological modelling of the East Greenland Caledonides – Isostatic support from crust and upper mantle, Tectonophysics (2016), http://dx.doi.org/10.1016/j.tecto.2016.06.023

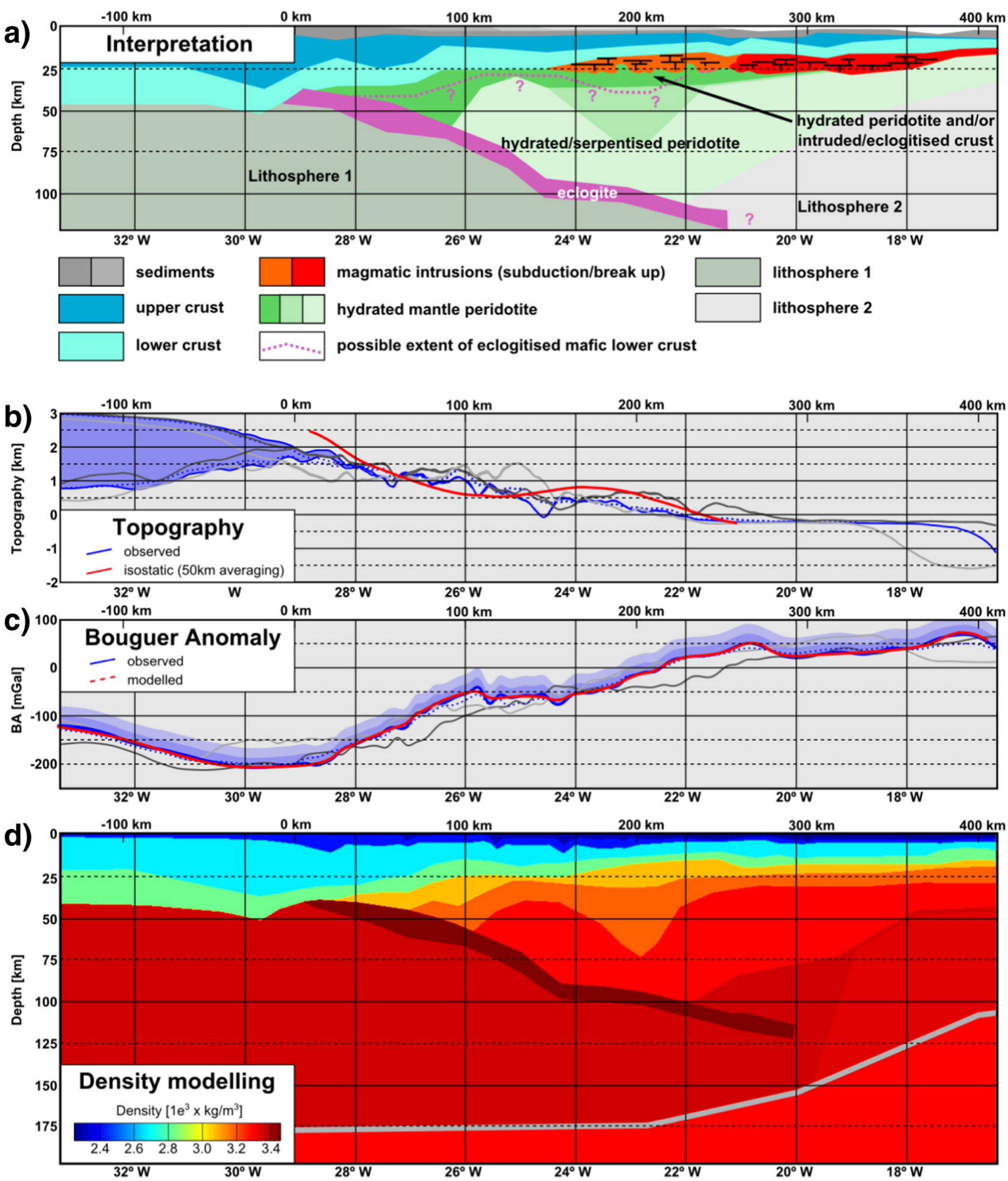

Fig. 9. Overview of the preferred interpretation and modelling results. (a) Simplified illustration showing the preferred model, including structures and their interpretation. (b) Topography. Blue – observed topography (50 km latitudinal average). Shaded blue area indicates the ice thickness. Stippled blue line – observed topography (100 km latitudinal average). Light grey – 50 km average topography south of the study profile. Dark grey line – 50 km average topography north of the study profile. Upper lines indicate ice topography, lower lines indicate bedrock topography. Red – isostatic topography using a running window of 50 km width to average the lithospheric density structure illustrated in d. (c) Bouguer anomaly (BA). Blue line – observed BA (50 km latitudinal average). Dotted blue line – observed BA (100 km latitudinal average). Light grey line: 50 km averaged BA, south of the profile. Dark grey line: 50 km averaged BA north of the study profile. Red – modelled BA from the lithospheric density structure illustrated in d. (d) Lithospheric density model giving rise to the modelled topography in b and BA in c. (For interpretation of the references to colour in this figure legend, the reader is referred to the web version of this article.)

and the structure of the crust and upper mantle are well explained by subduction related processes (Duesterhoeft et al., 2014). As argued in our previous studies, an early Caledonian east-dipping subduction, equivalent to the Grampian and Taconian phases in Britain and North America, respectively, is our preferred scenario. An earlier, e.g. Neoproterozoic origin (Cawood et al., 2010) or a younger, intra-cratonic subduction (Gilotti and McClelland, 2011), can also not be ruled out at this stage.

6. Conclusions

Receiver function analysis has revealed substantial heterogeneity and structure in the upper mantle of the Central Fjord region in East Greenland, including a dipping high velocity layer ($V_p > 8.3$ km/s) below a mantle wedge of intermediate velocities ($V_p = 7.3$–7.8 km/s). Detailed gravity and isostatic modelling corroborate this result. Further, petrological modelling of different compositions shows which lithologies may be associated with the observed velocities.

The most consistent models comprise alternating lower crustal bodies of intruded, mafic lower crust and serpentinised peridotite on top of a hydrated mantle wedge, and terminated at depth by a layer of eclogitised mafic crust. The crustal intrusions may be subduction related in the proximal margin domain, while break-up related intrusions may be expected in a more distal part of the margin, further east of the study area.

The models confirm that the lithosphere is close to isostatic compensation and therefore additional dynamic support from the sub-lithospheric mantle is limited. Our analysis showed that the crust of up to approximately 40 km thickness in the west of the profile is able to support the highest topography of 1000–1500 m, while the identified mantle wedge is accounting for additionally support of the topography in the east. Models including a homogeneous mantle lithosphere, lacking of a hydrated mantle wedge and a dipping eclogite layer, result in a poor fit, both of the gravity-isostatic models and the geophysical-petrological models.

In summary, our results support the existence of a fossil Caledonian subduction complex. The topography is isostatically supported from within the lithosphere. The implications of this for the bigger picture of the orogenic evolution and structural relations lie open for further discussions and testing.

Acknowledgements

The Central Fjord Array in East Greenland, the project and the production of this paper were part of the project “Topography of the North Atlantic Realm” (TOPOREAL, financed by the Danish Council for Independent Research (DFF). We thank DFF, all involved participants of TOPOREAL and all others who contributed to the discussion of the results. We want to thank Thorsten Nagel (Aarhus University), Folker Pappa and Erik Duesterhoeft (both Kiel University) for the help with the usage of Litmod2D, PERPL_EX and for productive discussions. The manuscript was finalised during C. Schiffer's Carlsberg Postdoctoral Fellowship at Durham University. We thank two anonymous reviewers for constructive comments.

References

Afonso, J.C., Fernàndez, M., Ranalli, G., Griffin, W.L., Connolly, J.a.D., 2008. Integrated geophysical-petrological modeling of the lithosphere and sublithospheric upper mantle: methodology and applications. Geochem. Geophys. Geosyst. 9 (5), Q05008. http://dx.doi.org/10.1029/2007GC001834.

Andersen, T.B., Jamtveit, B., Dewey, J.F., Swensson, E., 1991. Subduction and eduction of continental crust: major mechanisms during continent-continent collision and orogenic extensional collapse, a model based on the south Norwegian Caledonides. Terra Nova 3 (3), 303–310. http://dx.doi.org/10.1111/j.1365-3121.1991.tb00148.x.

Andersen, O.B., Knudsen, P., Berry, P.A.M., 2009. The DNSC08GRA global marine gravity field from double retracked satellite altimetry. J. Geod. 84 (3), 191–199. http://dx.doi.org/10.1007/s00190-009-0355-9.

Anderson, D.L., 2007. New Theory of the Earth. Cambridge University Press, Cambridge, UK ; New York.

Balling, N., 1980. The land uplift in Fennoscandia, gravity field anomalies and isostasy. In: Mörner, N.-A. (Ed.), Earth Rheology, Isostasy and Eustasy. Jon Wiley & Sons, New York, pp. 297–321.

Bamber, J.L., Griggs, J.A., Hurkmans, R.T.W.L., Dowdeswell, J.A., Gogineni, S.P., Howat, I., Mouginot, J., Paden, J., Palmer, S., Rignot, E., Steinhage, D., 2013. A new bed elevation dataset for Greenland. Cryosphere 7 (2), 499–510. http://dx.doi.org/10.5194/tc-7-499-2013.

Braitenberg, C., Wienecke, S., Ebbing, J., Born, W., Redfield, T., 2007. Joint gravity and isostatic analysis for basement studies - a novel tool. International Workshop, Innovation in EM, Grav and Mag Methods: A New Perspective for Exploration Extendended Abstracts.

Braun, A., Kim, H.R., Csatho, B., von Frese, R.R.B., 2007. Gravity-inferred crustal thickness of Greenland. Earth Planet. Sci. Lett. 262 (1–2), 138–158. http://dx.doi.org/10.1016/j.epsl.2007.07.050.

Brueckner, H.K., 2006. Dunk, dunkless and re-dunk tectonics: a model for metamorphism, lack of metamorphism, and repeated metamorphism of HP/UHP terranes. Int. Geol. Rev. 48 (11), 978–995. http://dx.doi.org/10.2747/0020-6814.48.11.978.

Brueckner, H.K., van Roermund, H.L.M., 2004. Dunk tectonics: a multiple subduction/eduction model for the evolution of the Scandinavian Caledonides. Tectonics 23 (2), TC2004. http://dx.doi.org/10.1029/2003TC001502.

Bryhni, I., Bollingberg, H.J., Graff, P.R., 1969. Eclogites in quartzo-feldspatic gneisses of Nordfjord, West Norway. Nor. Geol. Tidsskr. 49, 193–225.

Cawood, P.A., Strachan, R., Cutts, K., Kinny, P.D., Hand, M., Pisarevsky, S., 2010. Neoproterozoic orogeny along the margin of Rodinia: Valhalla orogen, North Atlantic. Geology 38 (2), 99–102. http://dx.doi.org/10.1130/G30450.1.

Chalmers, J.A., Green, P., Japsen, P., Rasmussen, E.S., 2010. The Scandinavian mountains have not persisted since the Caledonian orogeny. A comment on Nielsen et al. (2009a). J. Geodyn. 50 (2), 94–101. http://dx.doi.org/10.1016/j.jog.2010.02.001.

Christensen, N.I., 1996. Poisson's ratio and crustal seismology. J. Geophys. Res. Solid Earth 101 (B2), 3139–3156. http://dx.doi.org/10.1029/95JB03446.

Christensen, N.I., Mooney, W.D., 1995. Seismic velocity structure and composition of the continental crust: a global view. J. Geophys. Res. Solid Earth 100 (B6), 9761–9788. http://dx.doi.org/10.1029/95JB00259.

Cocks, L.R.M., Torsvik, T.H., 2011. The Palaeozoic geography of Laurentia and western Laurussia: a stable craton with mobile margins. Earth Sci. Rev. 106 (1–2), 1–51. http://dx.doi.org/10.1016/j.earscirev.2011.01.007.

Connolly, J.a.D., 1990. Multivariable phase diagrams; an algorithm based on generalized thermodynamics. Am. J. Sci. 290 (6), 666–718. http://dx.doi.org/10.2475/ajs.290.6.666.

Conrad, C.P., Lithgow-Bertelloni, C., 2006. Influence of continental roots and asthenosphere on plate-mantle coupling. Geophys. Res. Lett. 33 (5), L05312. http://dx.doi.org/10.1029/2005GL025621.

Corfu, F., Andersen, T.B., Gasser, D., 2014. The Scandinavian Caledonides: main features, conceptual advances and critical questions. Geol. Soc. Lond., Spec. Publ. 390, 9–43. http://dx.doi.org/10.1144/SP390.25.

Dahl-Jensen, T., Larsen, T.B., Woelbern, I., Bach, T., Hanka, W., Kind, R., Gregersen, S., Mosegaard, K., Voss, P., Gudmundsson, O., 2003. Depth to Moho in Greenland: receiver-function analysis suggests two Proterozoic blocks in Greenland. Earth Planet. Sci. Lett. 205 (3–4), 379–393. http://dx.doi.org/10.1016/S0012-821X(02)01080-4.

Darbyshire, F.A., Larsen, T.B., Mosegaard, K., Dahl-Jensen, T., Gudmundsson, Ó., Bach, T., Gregersen, S., Pedersen, H.A., Hanka, W., 2004. A first detailed look at the Greenland lithosphere and upper mantle, using Rayleigh wave tomography. Geophys. J. Int. 158 (1), 267–286. http://dx.doi.org/10.1111/j.1365-246X.2004.02316.x.

Deschamps, F., Godard, M., Guillot, S., Hattori, K., 2013. Geochemistry of subduction zone serpentinites: a review. Lithos 178, 96–127. http://dx.doi.org/10.1016/j.lithos.2013.05.019.

Dewey, J.F., 2005. Orogeny can be very short. Proc. Natl. Acad. Sci. 102 (43), 15286–15293. http://dx.doi.org/10.1073/pnas.0505516102.

Dewey, J.F., Ryan, P.D., Andersen, T.B., 1993. Orogenic uplift and collapse, crustal thickness, fabrics and metamorphic phase changes: the role of eclogites. Geol. Soc. Lond., Spec. Publ. 76 (1), 325–343. http://dx.doi.org/10.1144/GSL.SP.1993.076.01.16.

Doré, A.G., 2002. Exhumation of the North Atlantic Margin: Timing, Mechanisms and Implications for Petroleum Exploration. Geological Society of London.

Duesterhoeft, E., Quinteros, J., Oberhänsli, R., Bousquet, R., de Capitani, C., 2014. Relative impact of mantle densification and eclogitization of slabs on subduction dynamics: a numerical thermodynamic/thermokinematic investigation of metamorphic density evolution. Tectonophysics 637, 20–29. http://dx.doi.org/10.1016/j.tecto.2014.09.009.

Ebbing, J., 2007. Isostatic density modelling explains the missing root of the Scandes. Nor. J. Geol. 87, 13–20.

Ebbing, J., England, R.W., Korja, T., Lauritsen, T., Olesen, O., Stratford, W., Weidle, C., 2012. Structure of the Scandes lithosphere from surface to depth. Tectonophysics 536–537, 1–24. http://dx.doi.org/10.1016/j.tecto.2012.02.016.

Egholm, D.L., Nielsen, S.B., Pedersen, V.K., Lesemann, J.-E., 2009. Glacial effects limiting mountain height. Nature 460 (7257), 884–887. http://dx.doi.org/10.1038/nature08263.

Fichler, C., Odinsen, T., Rueslåtten, H., Olesen, O., Vindstad, J.E., Wienecke, S., 2011. Crustal inhomogeneities in the Northern North Sea from potential field modeling: inherited structure and serpentinites? Tectonophysics 510 (1–2), 172–185. http://dx.doi.org/10.1016/j.tecto.2011.06.026.

Fitton, J.G., Saunders, A.D., Norry, M.J., Hardarson, B.S., Taylor, R.N., 1997. Thermal and chemical structure of the Iceland plume. Earth Planet. Sci. Lett. 153 (3–4), 197–208. http://dx.doi.org/10.1016/S0012-821X(97)00170-2.

Forsberg, R., 1986. Gravity measurements in Jameson Land and neighbouring parts of East Greenland. Monogr. Greenl. Geosci. 253.

Forsberg, R., Kenyon, S., 2004. Gravity and geoid in the Arctic region - the northern polar gap now filled. ESA-ESRIN Proc. Second International GOCE User Workshop “GOCE, The Geoid and Oceanography.”.

Fossen, H., 2010. Extensional tectonics in the North Atlantic Caledonides: a regional view. Geol. Soc. Lond., Spec. Publ. 335 (1), 767–793. http://dx.doi.org/10.1144/SP335.31.

Foulger, G.R., Natland, J.H., Anderson, D.L., 2005. A source for Icelandic magmas in remelted Iapetus crust. J. Volcanol. Geotherm. Res. 141 (1–2), 23–44. http://dx.doi.org/10.1016/j.jvolgeores.2004.10.006.

Gaina, C., Werner, S.C., Saltus, R., Maus, S., 2011. Chapter 3 Circum-Arctic Mapping Project: New Magnetic and Gravity Anomaly Maps of the Arctic. Geol. Soc. Lond. Mem. 35 (1), 39–48. http://dx.doi.org/10.1144/M35.3.

Gasser, D., 2013. The Caledonides of Greenland, Svalbard and other Arctic areas: status of research and open questions. Geol. Soc. Lond., Spec. Publ. 390, 93–129. http://dx.doi.org/10.1144/SP390.17.

Gee, D.G., Fossen, H., Henriksen, N., Higgins, A.K., 2008. From the early Paleozoic platforms of Baltica and Laurentia to the Caledonide orogen of Scandinavia and Greenland. Episodes, Episodes.

Gernigon, L., Ringenbach, J.-C., Planke, S., Le Gall, B., 2004. Deep structures and breakup along volcanic rifted margins: insights from integrated studies along the outer Vøring Basin (Norway). Mar. Pet. Geol. 21 (3), 363–372. http://dx.doi.org/10.1016/j.marpetgeo.2004.01.005.

Gernigon, L., Blischke, A., Nasuti, A., Sand, M., 2015. Conjugate volcanic rifted margins, seafloor spreading and microcontinent: insights from new high-resolution aeromagnetic surveys in the Norway Basin. Tectonics http://dx.doi.org/10.1002/2014TC003717 (p. 2014TC003717).

Gilotti, J.A., McClelland, W.C., 2011. Geochemical and geochronological evidence that the North-East Greenland ultrahigh-pressure terrane is Laurentian crust. J. Geol. 119 (5), 439–456.

Gołędowski, B., Egholm, D.L., Nielsen, S.B., Clausen, O.R., McGregor, E.D., 2013. Cenozoic erosion and flexural isostasy of Scandinavia. J. Geodyn. 70, 49–57. http://dx.doi.org/10.1016/j.jog.2013.05.004.

Gradmann, S., Ebbing, J., Fullea, J., 2013. Integrated geophysical modelling of a lateral transition zone in the lithospheric mantle under Norway and Sweden. Geophys. J. Int. 194 (3), 1358–1373. http://dx.doi.org/10.1093/gji/ggt213.

Henriksen, N., 1999, Conclusion of the 1:500 000 mapping project in the Caledonian fold belt in North-East Greenland: Geology of Greenland Survey Bulletin, v. 183, p. 10–22.

Henriksen, N., and Higgins, A.K., 2008a, Caledonian orogen of East Greenland 70°N–82°N: geological map at 1:1,000,000—concepts and principles of compilation: Geological Society of America Memoirs, v. 202, p. 345–368, doi: 10.1130/2008.1202(14).

Henriksen, N., Higgins, A.K., 2008b. Geological research and mapping in the Caledonian orogen of East Greenland, 70°N–82°N. Geol. Soc. Am. Mem. 202, 1–27. http://dx.doi.org/10.1130/2008.1202(01).

Holland, T.J.B., Powell, R., 1998. An internally consistent thermodynamic data set for phases of petrological interest. J. Metamorph. Geol. 16 (3), 309–343. http://dx.doi.org/10.1111/j.1525-1314.1998.00140.x.

Jakobsson, M., Mayer, L., Coakley, B., Dowdeswell, J.A., Forbes, S., Fridman, B., Hodnesdal, H., Noormets, R., Pedersen, R., Rebesco, M., Schenke, H.W., Zarayskaya, Y., Accettella, D., Armstrong, A., et al., 2012. The International Bathymetric Chart of the Arctic Ocean (IBCAO) version 3.0. Geophys. Res. Lett. 39 (12), L12609. http://dx.doi.org/10.1029/2012GL052219.

Japsen, P., Chalmers, J.A., 2000. Neogene uplift and tectonics around the North Atlantic: overview. Glob. Planet. Chang. 24 (3–4), 165–173. http://dx.doi.org/10.1016/S0921-8181(00)00006-0.

Karabinos, P., Samson, S.D., Hepburn, J.C., Stoll, H.M., 1998. Taconian orogeny in the New England Appalachians: collision between Laurentia and the Shelburne Falls arc. Geology 26 (3), 215–218. http://dx.doi.org/10.1130/0091-7613(1998)026<0215:TOITNE>2.3.CO;2.

Kenyon, S., Forsberg, R., Coakley, B., 2008. New gravity field for the Arctic. EOS Trans. Am. Geophys. Union 89 (32), 289–290. http://dx.doi.org/10.1029/2008EO320002.

Korenaga, J., 2004. Mantle mixing and continental breakup magmatism. Earth Planet. Sci. Lett. 218 (3–4), 463–473. http://dx.doi.org/10.1016/S0012-821X(03)00674-5.

Kumar, P., Kind, R., Priestley, K., Dahl-Jensen, T., 2007. Crustal structure of Iceland and Greenland from receiver function studies. J. Geophys. Res. Solid Earth 112 (B3). http://dx.doi.org/10.1029/2005JB003991 (p. n/a–n/a).

Lachenbruch, A.H., Morgan, P., 1990. Continental extension, magmatism and elevation; formal relations and rules of thumb. Tectonophysics 174 (1–2), 39–62. http://dx.doi.org/10.1016/0040-1951(90)90383-J.

Leslie, A.G., Smith, M., Scoper, N.J., 2008. Laurentian margin evolution and the Caledonian orogeny - a template for Scotland and East Greenland. The Greenland CaledonidesGSA Memoirs Vol. 202. The Geological Society of America.

Lidmar-Bergström, K., Näslund, J.O., 2002. Landforms and uplift in Scandinavia. Geol. Soc. Lond., Spec. Publ. 196 (1), 103–116. http://dx.doi.org/10.1144/GSL.SP.2002.196.01.07.

Lundin, E.R., Doré, A.G., 2011. Hyperextension, serpentinization, and weakening: a new paradigm for rifted margin compressional deformation. Geology 39 (4), 347–350. http://dx.doi.org/10.1130/G31499.1.

Markl, G., Bucher, K., 1997. Proterozoic eclogites from the Lofoten islands, northern Norway. Lithos 42 (1–2), 15–35. http://dx.doi.org/10.1016/S0024-4937(97)00034-0.

Maupin, V., Agostini, A., Artemieva, I., Balling, N., Beekman, F., Ebbing, J., England, R.W., Frassetto, A., Gradmann, S., Jacobsen, B.H., Köhler, A., Kvarven, T., Medhus, A.B., Mjelde, R., et al., 2013. The deep structure of the Scandes and its relation to tectonic history and present-day topography. Tectonophysics 602, 15–37. http://dx.doi.org/10.1016/j.tecto.2013.03.010.

Medvedev, S., Hartz, E.H., 2015. Evolution of topography of post-Devonian Scandinavia: effects and rates of erosion. Geomorphology 231, 229–245. http://dx.doi.org/10.1016/j.geomorph.2014.12.010.

Medvedev, S., Souche, A., Hartz, E.H., 2013. Influence of ice sheet and glacial erosion on passive margins of Greenland. Geomorphology 193, 36–46. http://dx.doi.org/10.1016/j.geomorph.2013.03.029.

Miyashiro, A., Shido, F., Ewing, M., 1969. Composition and origin of serpentinites from the Mid-Atlantic Ridge near 24° and 30° North Latitude. Contrib. Mineral. Petrol. 23 (2), 117–127. http://dx.doi.org/10.1007/BF00375173.

Mjelde, R., Kasahara, J., Shimamura, H., Kamimura, A., Kanazawa, T., Kodaira, S., Raum, T., Shiobara, H., 2002. Lower crustal seismic velocity-anomalies; magmatic underplating or serpentinized peridotite? Evidence from the Vøring Margin, NE Atlantic. Mar. Geophys. Res. 23 (2), 169–183. http://dx.doi.org/10.1023/A:1022480304527.

Mjelde, R., Goncharov, A., Müller, R.D., 2013. The Moho: boundary above upper mantle peridotites or lower crustal eclogites? A global review and new interpretations for passive margins. Tectonophysics 609, 636–650. http://dx.doi.org/10.1016/j.tecto.2012.03.001.

Mørk, M.B.E., 1986. Coronite and eclogite formation in olivine gabbro (western Norway): reaction paths and garnet zoning. Mineral. Mag. 50 (3), 417–426.

Mysen, B.O., Heier, K.S., 1972. Petrogenesis of eclogites in high grade metamorphic gneisses, exemplified by the Hareidland eclogite, western Norway. Contrib. Mineral. Petrol. 36 (1), 73–94. http://dx.doi.org/10.1007/BF00372836.

Nielsen, S.B., Stephenson, R., Thomsen, E., 2007. Dynamics of Mid-Palaeocene North Atlantic rifting linked with European intra-plate deformations. Nature 450 (7172), 1071–1074. http://dx.doi.org/10.1038/nature06379.

Nielsen, S.B., Gallagher, K., Egholm, D.L., Clausen, O.R., Summerfield, M., 2009a. Reply to comment regarding the ICE-hypothesis. J. Geodyn. 48 (2), 101–106. http://dx.doi.org/10.1016/j.jog.2009.06.004.

Nielsen, S.B., Gallagher, K., Leighton, C., Balling, N., Svenningsen, L., Jacobsen, B.H., Thomsen, E., Nielsen, O.B., Heilmann-Clausen, C., Egholm, D.L., Summerfield, M.A., Clausen, O.R., Piotrowski, J.A., Thorsen, M.R., et al., 2009b. The evolution of western Scandinavian topography: a review of Neogene uplift versus the ICE (isostasy–climate–erosion) hypothesis. J. Geodyn. 47 (2–3), 72–95. http://dx.doi.org/10.1016/j.jog.2008.09.001.

Nirrengarten, M., Gernigon, L., Manatschal, G., 2014. Lower crustal bodies in the Møre volcanic rifted margin: geophysical determination and geological implications. Tectonophysics 636, 143–157. http://dx.doi.org/10.1016/j.tecto.2014.08.004.

Osmundsen, P.T., Ebbing, J., 2008. Styles of extension offshore mid-Norway and implications for mechanisms of crustal thinning at passive margins. Tectonics 27 (6), TC6016. http://dx.doi.org/10.1029/2007TC002242.

Pascal, C., Olesen, O., 2009. Are the Norwegian mountains compensated by a mantle thermal anomaly at depth? Tectonophysics 475 (1), 160–168. http://dx.doi.org/10.1016/j.tecto.2009.01.015.

Pedersen, V.K., Egholm, D.L., Nielsen, S.B., 2010. Alpine glacial topography and the rate of rock column uplift: a global perspective. Geomorphology 122 (1–2), 129–139. http://dx.doi.org/10.1016/j.geomorph.2010.06.005.

Peron-Pinvidic, G., Manatschal, G., Osmundsen, P.T., 2013. Structural comparison of archetypal Atlantic rifted margins: a review of observations and concepts. Mar. Pet. Geol. 43, 21–47. http://dx.doi.org/10.1016/j.marpetgeo.2013.02.002.

Reynisson, R.F., Ebbing, J., Lundin, E., Osmundsen, P.T., 2010. Properties and distribution of lower crustal bodies on the mid-Norwegian margin. Geol. Soc. Lond. Pet. Geol. Conf. Ser. 7, 843–854. http://dx.doi.org/10.1144/0070843.

Roberts, D., 2003. The Scandinavian Caledonides: event chronology, palaeogeographic settings and likely modern analogues. Tectonophysics 365 (1–4), 283–299. http://dx.doi.org/10.1016/S0040-1951(03)00026-X.

Rohrman, M., van der Beek, P., 1996. Cenozoic postrift domal uplift of North Atlantic margins: an asthenospheric diapirism model. Geology 24 (10), 901. http://dx.doi.org/10.1130/0091-7613(1996)024<0901:CPDUON>2.3.CO;2.

Rudnick, R.L., Gao, S., 2003. 3.01 - composition of the continental crust. In: Turekian, H.D.H.K. (Ed.), Treatise on Geochemistry. Pergamon, Oxford, pp. 1–64.

Rüpke, L.H., Schmid, D.W., Perez-Gussinye, M., Hartz, E., 2013. Interrelation between rifting, faulting, sedimentation, and mantle serpentinization during continental margin formation—including examples from the Norwegian Sea. Geochem. Geophys. Geosyst. 14 (10), 4351–4369. http://dx.doi.org/10.1002/ggge.20268.

Saunders, A.D., Fitton, J.G., Kerr, A.C., Norry, M.J., Kent, R.W., 1997. The North Atlantic Igneous Province. In: J.honey, J., Coffin, M.F. (Eds.), Large Igneous Provinces: Continental, Oceanic, and Planetary Flood Volcanism. American Geophysical Union, pp. 45–93.

Schiffer, C., Nielsen, S.B., 2016. Implications for anomalous mantle pressure and dynamic topography from lithospheric stress patterns in the North Atlantic Realm. J. Geodyn. 98, 53–69. http://dx.doi.org/10.1016/j.jog.2016.03.014.

Schiffer, C., Balling, N., Jacobsen, B.H., Stephenson, R.A., Nielsen, S.B., 2014. Seismological evidence for a fossil subduction zone in the East Greenland Caledonides. Geology 42 (4), 311–314. http://dx.doi.org/10.1130/G35244.1.

Schiffer, C., Jacobsen, B.H., Balling, N., Ebbing, J., Nielsen, S.B., 2015a. The East Greenland Caledonides—teleseismic signature, gravity and isostasy. Geophys. J. Int. 203 (2), 1400–1418. http://dx.doi.org/10.1093/gji/ggv373.

Schiffer, C., Stephenson, R.A., Petersen, K.D., Nielsen, S.B., Jacobsen, B.H., Balling, N., Macdonald, D.I.M., 2015b. A sub-crustal piercing point for North Atlantic reconstructions and tectonic implications. Geology 43 (12), 1087–1090. http://dx.doi.org/10.1130/G37245.1.

Schmidt, S., Götze, H.J., Fichler, C., Alvers, M., 2010. IGMAS + – a new 3D Gravity, FTG and Magnetic Modeling Software. Konferenzband GEO-INFORMATIK 2010 Die Welt im Netz, Herausgeber. Akademische Verlagsgesellschaft AKA GmbH, pp. 57–63.

Schmidt-Aursch, M.C., Jokat, W., 2005. The crustal structure of central East Greenland—II: from the Precambrian shield to the recent mid-oceanic ridges. Geophys. J. Int. 160 (2), 753–760. http://dx.doi.org/10.1111/j.1365-246X.2005.02515.x.

Skogseid, J., Planke, S., Faleide, J.I., Pedersen, T., Eldholm, O., Neverdal, F., 2000. NE Atlantic continental rifting and volcanic margin formation. Geol. Soc. Lond., Spec. Publ. 167 (1), 295–326. http://dx.doi.org/10.1144/GSL.SP.2000.167.01.12.

Smythe, D.K., Dobinson, A., McQuillin, R., Brewer, J.A., Matthews, D.H., Blundell, D.J., Kelk, B., 1982. Deep structure of the Scottish Caledonides revealed by the MOIST reflection profile. Nature 299 (5881), 338–340. http://dx.doi.org/10.1038/299338a0.

Snyder, D.B., Flack, C.A., 1990. A Caledonian age for reflectors within the mantle lithosphere north and west of Scotland. Tectonics 9 (4), 903–922. http://dx.doi.org/10.1029/TC009i004p00903.

Steltenpohl, M., Hames, W., Andresen, A., Markl, G., 2003. New Caledonian eclogite province in Norway and potential Laurentian (Taconic) and Baltic links. Geology 31 (11), 985–988. http://dx.doi.org/10.1130/G19744.1.

Streule, M.J., Strachan, R.A., Searle, M.P., Law, R.D., 2010. Comparing Tibet-Himalayan and Caledonian crustal architecture, evolution and mountain building processes. Geol. Soc. Lond., Spec. Publ. 335 (1), 207–232. http://dx.doi.org/10.1144/SP335.10.

Tegner, C., Lesher, C.E., Larsen, L.M., Watt, W.S., 1998. Evidence from the rare-earth-element record of mantle melting for cooling of the Tertiary Iceland plume. Nature 395 (6702), 591–594. http://dx.doi.org/10.1038/26956.

Thybo, H., Artemieva, I.M., 2013. Moho and magmatic underplating in continental lithosphere. Tectonophysics 609, 605–619. http://dx.doi.org/10.1016/j.tecto.2013.05.032.

van Staal, C.R., Whalen, J.B., Valverde-Vaquero, P., Zagorevski, A., Rogers, N., 2009. Pre-Carboniferous, episodic accretion-related, orogenesis along the Laurentian margin of the northern Appalachians. Geol. Soc. Lond., Spec. Publ. 327 (1), 271–316. http://dx.doi.org/10.1144/SP327.13.

Voss, M., Schmidt-Aursch, M.C., Jokat, W., 2009. Variations in magmatic processes along the East Greenland volcanic margin. Geophys. J. Int. 177 (2), 755–782. http://dx.doi.org/10.1111/j.1365-246X.2009.04077.x.

Warner, M., Morgan, J., Barton, P., Morgan, P., Price, C., Jones, K., 1996. Seismic reflections from the mantle represent relict subduction zones within the continental lithosphere. Geology 24 (1), 39–42. http://dx.doi.org/10.1130/0091-7613(1996)024<0039:SRFTMR>2.3.CO;2.

Xu, W., Lithgow-Bertelloni, C., Stixrude, L., Ritsema, J., 2008. The effect of bulk composition and temperature on mantle seismic structure. Earth Planet. Sci. Lett. 275 (1–2), 70–79. http://dx.doi.org/10.1016/j.epsl.2008.08.012.